Journal of Bioenergetics and Biomembranes, Vol. 27, No. 6, 1995

Control of Mitochondrial and Cellular Respiration by Oxygen

Erich Gnaiger,[1] Rosmarie Steinlechner-Maran,[1] Gabriela Méndez,[2] Thomas Eberl,[1] and Raimund Margreiter[1]

Received July 11, 1995

Control and regulation of mitochondrial and cellular respiration by oxygen is discussed with three aims: (1) A review of intracellular oxygen levels and gradients, particularly in heart, emphasizes the dominance of extracellular oxygen gradients. Intracellular oxygen pressure, p_{O_2}, is low, typically one to two orders of magnitude below incubation conditions used routinely for the study of respiratory control in isolated mitochondria. The p_{O_2} range of respiratory control by oxygen overlaps with cellular oxygen profiles, indicating the significance of p_{O_2} in actual metabolic regulation. (2) A methodologically detailed discussion of high-resolution respirometry is necessary for the controversial topic of respiratory control by oxygen, since the risk of methodological artefact is closely connected with far-reaching theoretical implications. Instrumental and analytical errors may mask effects of energetic state and partially explain the divergent views on the regulatory role of intracellular p_{O_2}. Oxygen pressure for half-maximum respiration, p_{50}, in isolated mitochondria at state 4 was 0.025 kPa (0.2 Torr; 0.3 μM O_2), whereas p_{50} in endothelial cells was 0.06–0.08 kPa (0.5 Torr). (3) A model derived from the thermodynamics of irreversible processes was developed which quantitatively accounts for near-hyperbolic flux/p_{O_2} relations in isolated mitochondria. The apparent p_{50} is a function of redox potential and protonmotive force. The protonmotive force collapses after uncoupling and consequently causes a decrease in p_{50}. Whereas it is becoming accepted that flux control is shared by several enzymes, insufficient attention is paid to the notion of complementary kinetic and thermodynamic flux control mechanisms.

KEY WORDS: Oxygen limitation; p_{50}; critical oxygen pressure; respirometry; polarographic oxygen sensor; human endothelial cells; rat liver mitochondria; intracellular p_{O_2}; oxygen gradients; kinetics; nonequilibrium thermodynamics.

INTRODUCTION

Oxygen levels in the cellular microenvironment must satisfy the kinetic and thermodynamic conditions for oxidative phosphorylation. Oxygen is supplied by intracellular diffusion to mitochondria, the final step in the respiratory cascade system (Weibel, 1984). Lack of oxygen leads to physiological and pathological consequences of hypoxia ranging from impairment of aerobic functions to ischemic injury and cell death. Understanding mitochondrial respiratory control by oxygen, therefore, is of fundamental importance to bioenergetics and of practical relevance in numerous clinical cases. However, compared with the attention paid to ADP, creatine or ion distribution, and membrane potential, few experimental studies address the role of oxygen for kinetic and thermodynamic regulation of cellular and mitochondrial respiration.

This discrepancy has several reasons. (1) Dependable techniques are rare for the measurement of oxygen kinetics in isolated mitochondria and cells. Resolution of oxygen levels in the kinetically relevant low range presents formidable instrumental and technical problems (Wilson *et al.*, 1988; Méndez and Gnaiger, 1994).

[1] Department of Transplant Surgery, University Hospital of Innsbruck, Anichstraße 35, A-6020 Innsbruck, Austria.

[2] Present address: Instituto de Investigaciones Cardiológicas, Universidad de Buenos Aires, 1122 Buenos Aires, Argentina.

0145-479X/95/1200-0583$07.50/0

The reason for contrasting results obtained by various laboratories is largely unresolved. (2) The affinity of cytochrome oxidase for oxygen is high, placing the oxygen dependence of mitochondrial respiration into the "microxic" domain of <1% air saturation. Therefore, zero-order kinetics of respiration in terms of oxygen is assumed under physiological conditions (Connett *et al.,* 1985; Wittenberg and Wittenberg, 1989; Gayeski and Honig, 1991), in which case metabolic regulation by oxygen would lack physiological significance. This view is not shared by others for either cardiac and skeletal muscle (Chance *et al.,* 1985; Jones, 1986; Chinet and Mejsnar, 1989; Rumsey *et al.,* 1990; Arthur *et al.,* 1992; Kreutzer and Jue, 1995). (3) The debate on oxygen levels and gradients in the cellular microenvironment is controversial. There is no doubt, however, that oxygen limitation of cellular energy metabolism plays a critical role in physiological and pathological states.

To address these issues, instrumental design and methodological considerations were combined to develop the technique of high-resolution respirometry for kinetic measurements at low oxygen in cultured cells (Steinlechner *et al.,* 1994) and isolated mitochondria (Méndez and Gnaiger, 1994). These studies provide a basis for the critical evaluation of respiratory control by oxygen and a new perspective on the relation between oxygen fluxes and thermodynamic forces under cellular hypoxia. This concept of thermodynamics of irreversible processes (TIP) incorporates the protonmotive force, the charge translocation stoichiometry of respiratory electron transport, and redox levels in the analysis of respiratory control by oxygen. The pronounced dependence of oxygen flux on oxygen pressure and near-hyperbolic relations are accounted for in the range <0.1 kPa, whereas less pronounced but significant effects of oxygen are expected at >0.1 kPa partial oxygen pressure. This is supported by experimental results. The standardized methodological approach of high-resolution respirometry and the conceptual basis of oxygen control provide a perspective for the application of oxygen kinetics as a diagnostic tool in the study of the physiological and pathological state of cells and mitochondria.

NORMOXIC p_{O_2} FROM AIR TO MITOCHONDRIA

The partial pressure, p_{O_2}, of air at sea level is approximately 20 kPa. Under these normoxic conditions, alveolar air contains oxygen of ca. 13 kPa. Oxygen diffuses to the blood which enters the lung at a mixed-venous p_{O_2} of 5 kPa (Weibel, 1984). Figure 1 summarizes the changes of p_{O_2} from capillary to mitochondria according to various authors (see legend, Fig. 1). A p_{O_2} difference of 2.7 kPa (20 torr) spans from the mean capillary p_{O_2} of 2.7–3.3 kPa to mitochondria of the working heart, and the steep part of the gradient is extracellular (Wittenberg and Wittenberg, 1989). Mitochondrial clusters may account for steep intracellular oxygen gradients (Jones, 1986). Intracellular myoglobin is near 50% oxygen saturation which is optimum for facilitated diffusion and thus supports high vectorial oxygen flux despite low oxygen gradients (Wittenberg and Wittenberg, 1985; Gayeski and Honig, 1991). Volume-averaged sarcoplasmic p_{O_2} is then 0.3 kPa (Wittenberg and Wittenberg, 1989) or 0.7 kPa (Gayeski and Honig, 1986) depending on the value used for half-saturating oxygen pressure of myoglobin at 37°C.

Oxygen gradients from capillary wall to mitochondria are nonlinear, steep in the periphery and shallow toward the center of a cell (Weibel, 1984; Gayeski and Honig, 1986; Dionne, 1990). Therefore, cellular oxygen profiles are presented on a logarithmic scale (Fig. 1). Ranges of respiratory oxygen control (horizontal bars; Fig. 1) are compared with the corresponding extracellular and intracellular oxygen levels (dashed and dotted lines; Fig. 1). Their overlap indicates the extent of actual oxygen regulation in the tissue. In the oxygen control range as defined in Fig. 1, respiratory flux is limited at 50–90% by p_{O_2} (horizontal bars). Extracellular and intracellular oxygen control ranges are distinguished since cellular respiration is sensitive to higher capillary than sarcolemmal p_{O_2}, corresponding to the p_{O_2} drop between these compartments. p_{50} is 0.02–0.06 kPa in isolated mitochondria under resting conditions (Table IA). This is equivalent to an intracellular 90% oxygen control range of 0.2–0.5 kPa (Fig. 1). At an intracellular p_{O_2} of 0.30 kPa and a p_{50} of 0.033 kPa, resting oxygen consumption is regulated to 90% owing to control by oxygen.

An opposite conclusion is drawn if reference is made to mitochondrial p_{50} <0.01 kPa (Table IB), in which case average intracellular oxygen concentrations of 0.3 kPa are not regulatory (Connett *et al.,* 1985; Wittenberg and Wittenberg, 1989). For resolving this discrepancy, evaluation of mitochondrial and cellular oxygen dependence is crucial, including detailed methodological considerations.

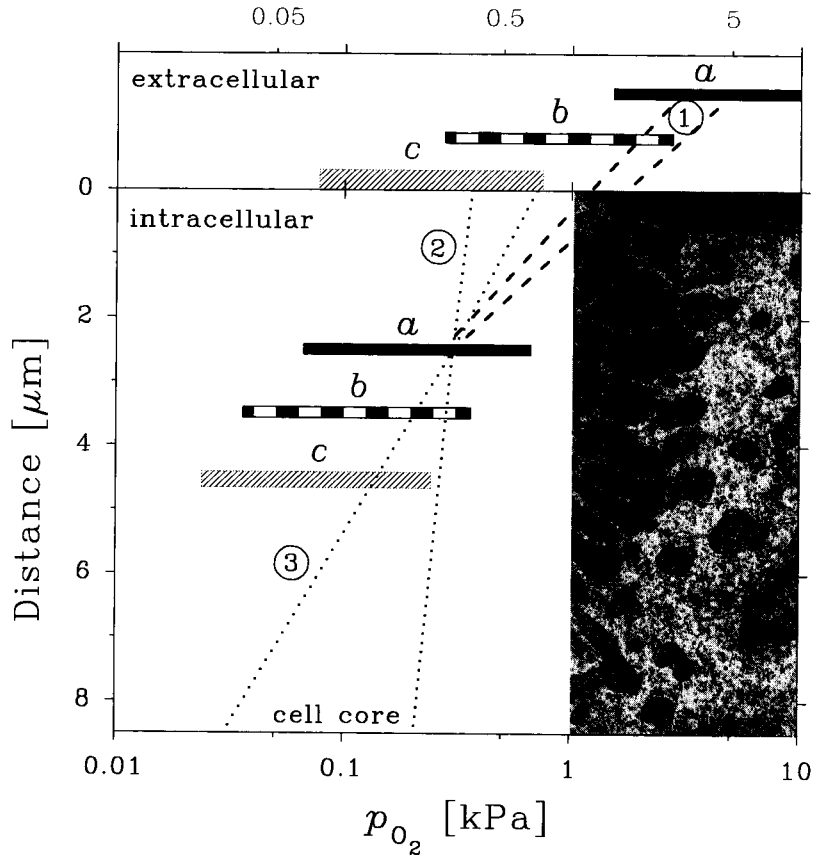

Fig. 1. Oxygen partial pressure, p_{O_2} [kPa], in the extracellular and intracellular microenvironment as a function of distance from the cell membrane. 8.5 μm is the radius of a typical cardiomyocyte where 50% of the volume is occupied in the cylinder from the membrane to 2.5 μm (level of bar *a*). The electron micrograph (Dr. G. Rieger) of the muscle cell shows myofibrils and mitochondria. Dashed lines (1) plot the extracellular–intracellular p_{O_2} difference, according to Wittenberg and Wittenberg (1989) with Δp_{O_2} = 2.7 kPa (shallow line), and according to Kreutzer and Jue (1995) [steeper line, from 5 to 0.3 kPa; Δp_{O_2} = 0.93 p_{O_2} (capillary) + 0.036]. Dotted lines represent very shallow (2) and moderately steep (3) intracellular oxygen gradients, corresponding to a p_{O_2} difference from cell membrane to core of 0.15 kPa (Dionne, 1990) and 0.67 kPa (Tamura *et al.*, 1989). For comparison, the horizontal bars show the oxygen control range where respiratory flux varies between 50 and 90% of oxygen-independent flux, measured as extracellular or intracellular p_{50} to p_{90}. Extension of the control range to cellular p_{O_2} levels indicates actual regulation of metabolic flux by oxygen. *a:* Perfused rat heart (Kreutzer and Jue, 1995). *b:* Isolated rat cardiomyocytes and isolated mitochondria (Rumsey *et al.*, 1990). *c:* Human endothelial cell cultures (Steinlechner *et al.*, 1994) and rat liver mitochondria in state 4 (Méndez and Gnaiger, 1994). The control range of endothelial cells is well below capillary p_{O_2} but overlaps with the intracellular oxygen gradients extrapolated to the capillary wall.

RESPIROMETRIC MEASUREMENT OF OXYGEN DEPENDENCE

Oxygen affinities of cells and mitochondria are summarized in Table I. Extracellular p_{50} values depend on cell type and metabolic activity and are 5–10 times above the mitochondrial p_{50}. When arranging the studies according to methods (A) without gas phase and (B) with steady-state oxygen transfer from a gas phase into the aqueous incubation medium, results with the latter methods tend to yield p_{50} values one order of magnitude lower. Oxygen transfer between a gaseous

Table I. Respiratory Control by Oxygen in Cells and Mitochondria in Various Metabolic States. A. Respirometric measurements independent of gaseous–aqueous phase transition of O_2. B. Measurements based on steady-state or near-steady state transfer of O_2 from gaseous to aqueous phases. p_{50} [kPa; 1 mm Hg = 0.133322 kPa] is reported for the extracellular (A.1 and B.1) or intracellular space and mitochondrial incubation media (A.2 and B.2). Maximum control fluxes, J_{max}, are expressed per 10^6 cells or per dry weight, as indicated by the unit *x*. The measuring apparatus and oxygen sensor are indicated (polarographic oxygen sensor, POS).

System	T (°C)	State	p_{50} (kPa)	J_{max} (pmol·s^{-1}/unit *x*)		Measurement (reference)
A.1. Extracellular p_{50}						Respirometry without gas phase
Human umbilical vein endothelial cell culture, growth medium M199	37	Coupled	0.094	20	10^6 cells	Oroboros Oxygraph, POS (Steinlechner *et al.*, 1994)
Human umbilical vein endothelial cell culture, growth medium EGM	37	Coupled	0.063	45 45	10^6 cells mg dry weight	Oroboros Oxygraph, POS (Steinlechner *et al.*, 1994)
		Uncoupled	0.10	110	10^6 cells	
		Uncoupled, inhibited	0.023	35	10^6 cells	Oroboros Oxygraph, POS (Fig. 3)
Rat coronary endothelial cell culture	37	Glucose	0.11	65	mg protein	Steady-state injection, POS (Mertens *et al.*, 1990)
		Palmitate, glutamine	0.11	130	mg protein	
Rat heart, mean end capillary p_{O_2}	25	Perfused heart	1.60	160	mg dry weight	Perfusion system, POS (Kreutzer and Jue, 1995)
Rat cardiac myocytes	25[a]	Resting	0.19	220	mg dry weight[b]	Closed, phosphorescence (Rumsey *et al.*, 1990)
		$+Ca^{2+}$	0.29	250	mg	
		Uncoupled	0.79	2120	mg	
		Uncoupled, inhibited	0.10	190	mg	
Rat cardiac myocytes	31		0.32	1290 195	10^6 cells mg protein	O_2 pulses, reduction time of cyt $a + a_3$ (Kennedy and Jones, 1986)
Isolated hepatocytes	37		0.25	170 250	mg protein 10^6 cells	Closed, POS (Jones and Mason, 1978)
Isolated hepatocytes	29		0.27	220	10^6 cells	O_2 pulses, reduction time of cyt $c + c_2$ (Jones and Kennedy, 1982)
Neuroblastoma cell cultures	?	Coupled	0.11	75	mg dry weight	Closed, phosphorescence (Robiolio *et al.*, 1989)
		Uncoupled	0.09	355	mg	
		Uncoupled, inhibited	0.02	75	mg	
Ascites tumor cells	25	Ascorbate, TMPD, valinomycin	0.17	1770	mg protein	Closed, POS (Ferreira, 1992)
A.2. Mitochondrial p_{50}						Respirometry without gas phase
Rat heart, intracellular p_{O_2}	25	Perfused heart	0.070	160	mg dry weight	Intracellular myoglobin saturation, $p_{50,Mb}$ = 0.20 kPa (Kreutzer and Jue, 1995)
Rat cardiac myocytes, intracellular p_{O_2}	30	Coupled	0.015	91 370	mg protein 10^6 cells	Intracellular myoglobin saturation,[c] $p_{50,Mb}$ = 0.17 kPa (Wittenberg and Wittenberg, 1985)
		Uncoupled	0.029	305 1250	mg protein 10^6 cells	

Table I. Continued

System	T (°C)	State	p_{50} (kPa)	J_{max} (pmol·s^{-1}/unit x)	Measurement (reference)
Rat heart mitochondria, 0.2–0.8 μM cyt c	25[a]	State 4, glutamate, malate	0.038	570 nmol cyt c	Closed, phosphorescence (Rumsey *et al.*, 1990)
		State 4, glutamate, succinate, malate	0.048	1230 nmol cyt c	
0.11 mg protein·cm^{-3}		Uncoupled	0.014	1730 mg protein	
0.05 mg protein·cm^{-3}		Uncoupled, dilute	0.005	1130 mg protein	
Rat skeletal muscle mitochondria	37	State 4, glutamate malate	0.025	170 cm^3 medium	Oroboros Oxygraph, POS (unpublished)
Rat liver mitochondria, 0.2–0.6 mg protein·cm^{-3}	25	State 4, succinate, rotenone	0.025	210 mg protein	Oroboros Oxygraph, POS (Méndez and Gnaiger, 1994; and unpublished)
Rat liver mitochondria, 1 mg protein·cm^{-3}	25[a]	State 4, succinate, glutamate	0.06	670 mg protein	Closed, phosphorescence (Wilson *et al.*, 1988)
		Uncoupled	<0.007	6000 mg protein	
B.1. Extracellular p_{50}					Respirometry with gas phase
Rat cardiac myocytes	30	Resting	0.016	370 10^6 cells	POS (Wittenberg and Wittenberg, 1985)
		Uncoupled	0.11	1250 10^6 cells	
B.2. Mitochondrial p_{50}					Respirometry with gas phase
Rat skeletal muscle mitochondria, 10 mg protein·cm^{-3}	25	State 3, glutamate, malate	0.005	1500 mg protein	POS (Cole *et al.*, 1982)
Pigeon heart mitochondria, 0.2 mg protein·cm^{-3}	25	State 4, succinate, glutamate	0.008[d]	530 mg protein	Bacterial luminescence (Sugano *et al.*, 1974)
		State 3	0.08[d]	2900 mg protein	
Rat liver mitochondria, 6 mg protein·cm^{-3}	?	Coupled, pyruvate, malate	0.05	110 mg protein	Vibrating platinum electrode (Degn and Wohlrab, 1971)
		Uncoupled	<0.005		

[a] Experimental temperature and oxygen solubility of 12.0 μM·kPa^{-1} inferred from Dionne (1990).
[b] The authors report 13.22 nmol O_2·min^{-1}·g^{-1} dry weight (coupled cells) and 127.0 nmol O_2·min^{-1}·g^{-1} dry weight (uncoupled cells), but per mg is probably the correct unit.
[c] Oxygen flux was measured in a respirometer with a gas phase (compare Table IB), but the p_{O_2} was measured intracellularly.
[d] Calculated from the p_{O_2} at half-maximal reduction of cytochrome c, and the oxygen flux at this p_{50_c}.

and aqueous phase gives rise to potential problems of unstirred boundary layers and oxygen gradients between O_2 exchange and O_2 sensor, particularly in systems with very high volume-specific oxygen flux (mitochondrial concentration times mass-specific flux; Table I). The importance of such gradients is indicated by the observation that the spectrophotometric signal for cytochromes $a + a_3$ at steady state reaches up to 50% oxidation when the oxygen signal measured in the aqueous phase is essentially zero (Petersen *et al.*, 1974).

Interference of gas–liquid phase transitions is circumvented in closed aqueous-phase respirometers. Technical specifications of respirometers for the measurement at low p_{O_2} require the prevention of uncontrolled oxygen diffusion, stability of the signal at high and low oxygen, minimization of oxygen diffusion fields, and sufficient time resolution of the system (Schindler, 1967). The solution, however, does not solely reside in improvements of the measuring instrument but in a combination of careful methodological control experiments and mathematical signal correction.

An Oxygraph for High-Resolution Respirometry

Classical Oxygraph chart recorder traces are impractical for appropriate data analysis. On the basis

of digital data acquisition, signal corrections can account for (1) the time response of the oxygen sensor, (2) oxygen leak and blank oxygen consumption, and (3) time-dependent zero drift of the oxygen sensor. Thereby, the limitations ascribed to the polarographic oxygen sensor (Wilson *et al.*, 1988) are overcome and combined with the convenience of a readily available respirometric system. A two-channel titration–injection respirometer was developed for high-resolution respirometry (Oroboros Oxygraph, Paar KG, Graz, Austria) and applied to the study of the oxygen dependence of isolated mitochondria and cultured cells (Méndez and Gnaiger, 1994; Steinlechner *et al.*, 1994).

The sensitivity of polarographic oxygen sensors is a function of cathode area (Hale, 1983). The signal-to-noise ratio increases and the relative signal drift at zero oxygen decreases with cathode diameter (Cole *et al.*, 1982). Therefore, a polarographic oxygen sensor (Orbisphere Model 2120) was chosen with a relatively large cathode (2 mm diameter). The angular insertion of the sensor to the glass chamber (Haller *et al.*, 1994) places the cathode into an optimum position for stirring, contrary to centrally inserted cathodes which are at the point of minimum water current. Stirring rates of 6 or 8 rotations per second (350 rpm for cells, 500 rpm for mitochondria) are sufficient and yield similar time constants. Noise is reduced with decreasing oxygen to less than ±0.003 kPa, which is of particular advantage for measurements at low p_{O_2} (Fig. 2).

Signal Correction for Response Time and Blank Controls

The response of polarographic oxygen sensors to a step change in p_{O_2} is exponential (Hale, 1983). The time constant, τ, is determined experimentally and used for correcting the raw signals, c_{raw},

$$c_{O_2} = c_{raw} + \tau \frac{dc_{raw}}{dt} \qquad (1)$$

where c_{O_2} is the actual oxygen concentration at time t (s). With well-maintained sensors, τ is 4–3 s at 25–37°C, but smoothing distorts the time resolution when a moving average is applied over the oxygen-dependent range. Oxygen dependence based on raw data is overestimated significantly (Starlinger and Luebbers, 1972), but this artefact can be quantitatively eliminated [Eq. (1)].

Uncontrolled oxygen diffusion into the aqueous phase must be minimized by appropriate choice of materials in contact with the incubation medium. A high oxygen leak from commonly used Teflon-coated stirrers is expected in rapid aerobic–anaerobic transitions, since the O_2 solubility of Teflon is 106 $\mu M \cdot kPa^{-1}$ at 25°C (Hale, 1983) compared to 11 $\mu M \cdot kPa^{-1}$ in typical mitochondrial incubation media (Reynafarje *et al.*, 1985). The standard Teflon stirrer bar functions as an oxygen reservoir which gives off oxygen at low p_{O_2}, up to −30 pmol $O_2 \cdot s^{-1} \cdot cm^{-3}$ when oxygen is lowered quickly (Haller *et al.*, 1994). Such an oxygen leak distorts any measurement of mitochondrial oxygen dependence, since 50–200 $pmol \cdot s^{-1} \cdot cm^{-3}$ are typical oxygen fluxes at state 4 with mitochondrial protein concentrations of 0.2–1 $mg \cdot cm^{-3}$ (Table I). In a recent study of the oxygen dependence of cellular respiration with a Teflon-coated stirrer (Rumsey *et al.*, 1990), a rate of back-diffusion of −5 $pmols \cdot s^{-1} \cdot cm^{-3}$ was reported (Robiolio *et al.*, 1989). This is 3–10 times higher than in the Oroboros Oxygraph where PEEK-coated stirrers are used (Fig. 2). Despite the careful choice of all materials in contact with the medium (glass chambers, titanium stoppers, viton O-rings, PEEK stirrers), back-diffusion at zero oxygen amounts to −0.5 to −1.5 $pmol \cdot s^{-1} \cdot cm^{-3}$ with chamber volumes of 2–3 cm^3 (Fig. 2B). This oxygen stems most likely from unstirred boundary layers in the measuring chamber and the electrolyte reservoir of the polarographic oxygen sensor. After anoxia over several hours, these stores are depleted and back-diffusion is absolutely zero over days.

While quantitative reports on back-diffusion are scarce, corrections for this effect are hardly ever reported for closed systems (for perfusion systems see Gnaiger, 1983; Kreutzer and Jue, 1995). Blank control oxygen flux, measured at stepwise reduced p_{O_2} in the absence of biological sample, is the net result of sensor oxygen consumption and back-diffusion. Oxygen consumption by the polarographic oxygen sensor increases linearly with oxygen pressure, whereas the counter-effective back-diffusion is maximum at zero oxygen and after rapid aerobic–anoxic transitions (Fig. 2B). Oxygen concentration declines continuously in the closed respirometer, and blank-corrected oxygen consumption, J_{O_2} ($pmol \cdot s^{-1} \cdot cm^{-3}$), is calculated as

$$J_{O_2} = -dc_{O_2}/dt \cdot 1000 - (a^\circ + b^\circ \cdot c_{O_2}) \qquad (2)$$

where c_{O_2} ($nmol \cdot cm^{-3}$) is oxygen concentration measured at time t [Eq. (1)], dc_{O_2}/dt is the time derivative of oxygen concentration, and the expression in parentheses is $J^\circ_{O_2}$, the blank-control oxygen flux. a° ranged from −0.5 to −2.5 $pmol \cdot s^{-1} \cdot cm^{-3}$, and b° was typi-

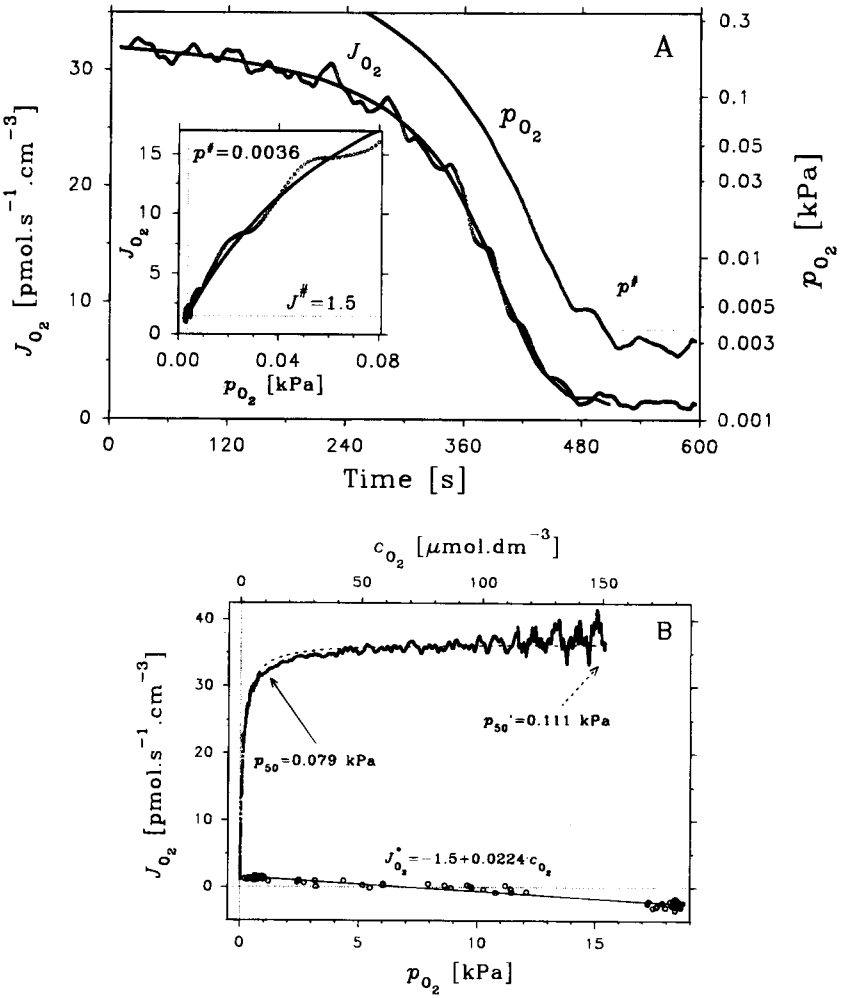

Fig. 2. Closed-chamber respirometry and oxygen dependence of a human umbilical vein endothelial cell culture. A. Decline of oxygen flux, J_{O_2} (pmol · s^{-1} · cm^{-3}) (○), and p_{O_2} (kPa) (●) with time. Individual data points recorded at 1-s intervals merge partially to give the appearance of a full line. The full line, J_{O_2}, shows the hyperbolic fit in the range 0.0036 kPa < p_{O_2} < 1.1 kPa (B) as a function of time. p_{O_2} is plotted on a logarithmic scale in the range up to 75% of maximum flux (three times p_{50}', B). Inset: Oxygen flux as a function of oxygen pressure, p_{O_2}, in the range below p_{50}. The full line shows the hyperbolic fit. The dotted lines are $J^\#$ and $p^\#$ crossing at the compensation point. $p^\#$ cannot be determined from a p_{O_2}/time plot shown in the main figure, where $p^\#$ indicates the time beyond which data are cut off for further data analysis; residual signal change is due to zero drift. B. Oxygen flux, J_{O_2}, as a function of oxygen pressure, p_{O_2} (kPa), or oxygen concentration, c_{O_2} [µM]. Arrows point to the p_{O_2} below which data were included for hyperbolic fits shown by dashed line (full p_{O_2} range, yielding half-maximum flux at p_{50}') and full line (low p_{O_2} range < 1.1 kPa). The dependence of the calculated p_{50} on the O_2 range indicates a deviation from hyperbolic relationships. Open symbols and full line are plots of the negative blank control values of the Oxygraph, $-J^\circ_{O_2} = -(a^\circ + b^\circ \cdot c_{O_2})$, as used for blank control correction [Eq.(2)]. The intercept of the hyperbolic kinetics of cells and the linear relation of the blank controls is the compensation point at which a minimum cellular oxygen flux is compensated by oxygen diffusion, $J^\# = 1.5$ pmols · s^{-1} · cm^{-3}, at a constant minimum p_{O_2} (inset of Fig. 2A). 2 cm^3 chamber volume; 0.78 · 10^6 cells · cm^{-3} in endothelial cell growth medium; 37°C.

cally 0.02–0.03 s^{-1}, corresponding to $J^{\circ}_{O_2}$ of 3–4 $pmol \cdot s^{-1} \cdot cm^{-3}$ at air saturation owing to electrochemical oxygen reduction at the cathode.

Acquisition of averaged data points in 1-s intervals was adequate, although a higher sampling rate at 200 ms time intervals is possible. A specific data acquisition and analysis software was developed which routinely includes signal deconvolution with calibrated time constants and blank control correction [Eqs. (1) and (2); DatLab; Oroboros, Innsbruck, Austria].

Internal Zero Calibration

High concentrations of mitochondria or submitochondrial particles deplete oxygen practically to zero in a closed respirometer, providing a convenient zero calibration (Méndez and Gnaiger, 1994). At lower concentrations of coupled mitochondria and cells, however, oxygen is depleted to a minimum of $c^{\#}$ or $p^{\#}$ (concentration or pressure; Fig. 2A). $p^{\#}$ can be calculated from the intercept of the hyperbolic respiratory function and the linear slope of the blank controls (Fig. 2B). At this compensation point, oxygen concentration is constant with time, $dc_{O_2}/dt = 0$, when respiratory flux, $J^{\#}$, just compensates for back-diffusion, a° [Eq. (2)].

Accuracy of measurements at p_{O_2} <0.02 kPa (<0.1% air saturation) is limited owing to potential zero drift of the oxygen sensor. However, internal zero oxygen calibration is possible in each aerobic–anaerobic transition with information on $p^{\#}$, increasing the resolution of oxygen measurements by two orders of magnitude (Fig. 2A). In a first iteration, $p^{\#}$ is set to 0 kPa and this value used for internal zero calibration. The near-hyperbolic flux/p_{O_2} relation yields a first approximation of J_{max} and p_{50},

$$J_{O_2} = \frac{J_{max} \cdot p_{O_2}}{p_{50} + p_{O_2}} \qquad (3)$$

Inserting $J^{\#} \approx -a^{\circ}$ into Eq. (3), we calculate $p^{\#}$:

$$p^{\#} = \frac{p_{50} \cdot J^{\#}}{J_{max} - J^{\#}} \qquad (4)$$

This new value is used for a final correction of the internal zero oxygen calibration. The recalibrated p_{O_2} values are then the basis for fitting the hyperbolic parameters in a second iteration (inset Fig. 2A). $p^{\#}$ increases linearly with the p_{50}/J_{max} ratio as long as back-diffusion is low in relation to J_{max} [Eq. (4)]. Results of zero fluxes or zero oxygen concentrations are inconsistent when obtained in experiments with high $-a^{\circ}/J_{max}$ ratios and indicate errors in zero oxygen calibration.

Critical p_{O_2}, p_{50}, and Near-Hyperbolic p_{O_2} Dependence

The p_{50} is an index for the oxygen affinity of the respiratory system [Eq. (3)]. Considering that oxygen limitation by a few percent may be physiologically relevant, oxygen dependence is frequently described by a critical oxygen pressure, p_c, below which respiratory function is significantly impaired. Significance in this case is evaluated from a physiological and not merely statistical perspective. For example, critical levels, c, were considered as 75, 80 or 90% of J_{max} in different contexts by Gnaiger (1993a), Kreutzer and Jue (1995), and Jöbsis (1972), respectively. The corresponding p_c values are 3, 4, and 9 times higher than the p_{50}, if a hyperbolic relation [Eq. (3)] is assumed,

$$\frac{p_c}{p_{50}} = \frac{c}{100 - c} \qquad (5)$$

p_{50} values provide a convenient basis for general comparison (Table I). However, regulation of oxygen must be evaluated in terms of p_c in relation to intracellular p_{O_2} (Fig. 1).

Flux/p_{O_2} relations of mitochondrial or cellular respiration correspond to hyperbolic or near-hyperbolic functions, although significant deviations are reported (Petersen *et al.*, 1974; Froncisz *et al.*, 1985). Different p_{50} values are obtained when various oxygen ranges are selected for hyperbolic fitting depending on (1) deviations from the hyperbolic function, (2) the distribution of data points and noise over the oxygen range, and (3) the choice between nonlinear curve fitting versus linear regression analysis of transformed data (e.g., double reciprocal Lineweaver–Burk plots). For example, an apparent p_{50}' of 0.11 kPa was obtained in a typical experiment with endothelial cells when the full range from air saturation to zero oxygen was included in a nonlinear fit, but the p_{50} was 30% lower when considering the range <1 kPa (Fig. 2B; a similar trend was observed in isolated mitochondria). A Lineweaver–Burk regression analysis over the entire range gave a still lower p_{50} of 0.06 kPa. Double reciprocal regression is comparatively insensitive to variations in the high-oxygen range but highly sensitive to noise

at low p_{O_2}. Nonlinear curve fitting is mandatory for statistical reasons. Data points must be cut off as soon as the compensation point is reached to avoid distortion of curve fitting by an accumulation of data at the lowest values and to exclude the effect of zero drift (Fig. 2A). A standard oxygen range <1.1 kPa is recommended, covering a range from 10 to 100 times the p_{50}. Apart from statistics, the respirometric data at high oxygen may include effects of incubation time and respond to mechanisms operative in a different kinetic domain (Schumacker *et al.*, 1993).

In summary, several potential artifacts must be carefully excluded in the measurement of mitochondrial respiratory control by oxygen. A crucial test for appropriate measuring conditions and correct data analysis is the variation of mitochondrial density (Rumsey *et al.*, 1990), which changes the volume-specific J_{max} but should be without effect on the p_{50}. The p_{50} of isolated rat liver mitochondria was independent of protein concentration in the entire range of 0.2–0.6 mg·cm^{-3} tested in the Oroboros Oxygraph (Méndez and Gnaiger, 1994).

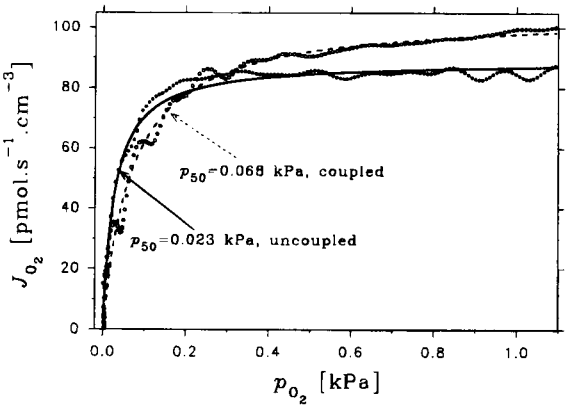

Fig. 3. Oxygen flux, J_{O_2} (pmol · s^{-1} · cm^{-3}), of coupled (open circles) and uncoupled (closed circles) human umbilical vein endothelial cells, at similar maximum fluxes of 104 and 89 pmol · s^{-1} · cm^{-3}, respectively, both at 2.6 · 10^6 cells · cm^{-3}. Cells were uncoupled and inhibited by a high concentration of the protonophore FCCP (6 μmol · dm^{-3}). The hyperbolic fits are shown by the dashed line (coupled) and full line (uncoupled). 2 cm^3 chamber volume; endothelial cell growth medium; 37°C.

EFFECT OF DIFFUSION GRADIENTS AND ENERGETIC STATE ON p_{50}

Differences of extracellular and intracellular p_{50} reflect oxygen gradients between the extracellular space and mitochondrion (Fig. 1). In addition, differences of p_{50} based on intracellular oxygen probes or measured with isolated mitochondria reveal specific effects of metabolic state on oxygen affinity. If diffusion limitation predominates, a semilogarithmic plot of oxygen pressure as a function of time should be linear in the low range (Froncisz *et al.*, 1985). A hyperbolic fit was clearly superior to the semilogarithmic plot for endothelial cells (Fig. 2), in contrast to results on Chinese hamster ovary cells (Froncisz *et al.*, 1985). The p_{50} of human umbilical vein endothelial cells respiring in growth medium (0.06–0.09 kPa; Fig. 3) compares well with the p_{50} of rat coronary endothelial cells (0.11 kPa; Mertens *et al.*, 1990). Isolated endothelial cells have a lower p_{50} than cardiac myocytes, but the extracellular p_{50} values of coupled cells (Figs. 2 and 3) are higher than the p_{50} of mitochondria in state 4 (Fig. 4). Oxygen regulation of endothelial metabolism depends on the actual oxygen profile from erythrocyte to the tissue (Fig. 1), and on the possible role of nitric oxide production and competitive inhibition of cytochrome *c* oxidase by NO (Brown and Cooper, 1994).

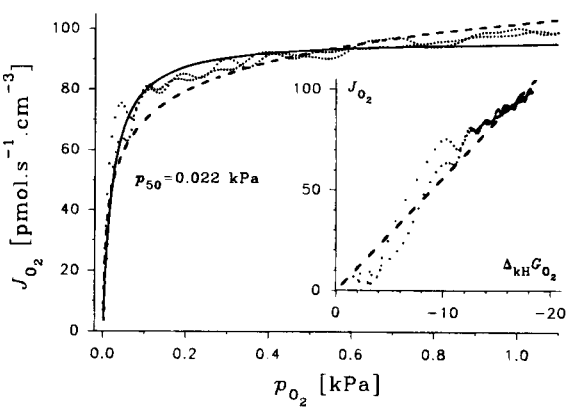

Fig. 4. Hyperbolic oxygen flux/pressure relation in isolated rat liver mitochondria in the transition from state 4 to state 5. J_{O_2} is expressed per volume of the Oxygraph chamber (3 cm^3; 0.47 mg mitochondrial protein per cm^3). Two replica from an identical preparation are superimposed. Each dot represents a data point sampled at 1-s intervals. Calculations are carried out for the combined data. Full line: hyperbolic fit; p_{50} = 0.022 kPa; J_{max} = 0.21 pmol · s^{-1} · mg^{-1} mitochondrial protein. Dashed line: fit according to Eq. (12); $\Delta_{kH}G^*_{O_2}$ = −18.1 kJ · mol^{-1}; L = 5.6 pmol^2 · s^{-1} · cm^{-3} · nJ^{-1}. Inset: Linear flux/force relation, plotted on the basis of $\Delta_{kH}G^*_{O_2}$ = −18.1 kJ · mol^{-1} and Eq. (12). One data set from Méndez and Gnaiger (1994). Medium composition: 0.23 M sucrose, 0.5 mM EGTA, 3.0 mM K$^+$HEPES, 11 mM $MgCl_2$, 5.0 mM K$^+$succinate, 5 μM rotenone, 1.5 mg/ml fatty acid free BSA, 1.9 mM ATP, 10 mM KH_2PO_4, pH 7.35, 25°C.

The effect of "energization" is an outstanding feature of mitochondrial oxygen kinetics (Chance, 1965; Degn and Wohlrab, 1971; Petersen *et al.*, 1974). This is expected when considering cytochrome *c* oxidase as a redox-linked proton pump (Babcock and Wikström, 1992; Malmström, 1993; Einarsdóttir, 1995). The mitochondrial p_{50} is not a Michaelis–Menten *constant* but depends on metabolic state, increasing from 0.01 kPa at state 4 (high ATP) to 0.1 kPa at state 3 (high ADP; Chance *et al.*, 1985). Using this p_{50} for state 3, the critical p_{O_2} at 90% would be as high as 0.9 kPa in skeletal muscle working at maximum aerobic capacity, while < 0.1 kPa is reported as the upper bound for the p_c *in vivo* (Connett *et al.*, 1985). In the latter case, the mitochondrial p_{50} at state 3 would be equal to or less than p_{50} at state 4. This trend is observed in uncoupled mitochondria where p_{50} decreases to extremely low levels (Table I). Similar to the situation in isolated cardiomyocytes (Rumsey *et al.*, 1990), stimulation of respiration by uncoupling endothelial cells increases p_{50} under the control of oxygen gradients (Steinlechner *et al.*, 1994). In contrast, inhibited uncoupled cells have a lower p_{50} compared to coupled cells (Fig. 3). This reflects the complex interaction of diffusion gradients and metabolic states on respiratory control by oxygen.

Two replica of an experiment with isolated rat liver mitochondria in the transition from state 4 to state 5 are shown superimposed in Fig. 4. The hyperbolic fit yields an apparent p_{50} of 0.022 kPa, representative of the average p_{50} of 0.025 ± 0.006 kPa (mean ± SE; six independent experiments; Méndez and Gnaiger, 1994).

Kinetic and near-equilibrium models have been discussed to account for the effect of metabolic state on respiratory control by oxygen (Wilson *et al.*, 1979b; Chance *et al.*, 1985). Alternatively, allosteric control of cytochrome *c* oxidase has been implied, including the membrane potential among the possible allosteric effectors (Kadenbach, 1986; Nicholls, 1993). In the following section, a concept using the thermodynamics of irreversible processes is presented to account for the effects of redox potential and protonmotive force (and phosphorylation potential in turn) on the oxygen dependence of mitochondrial respiration.

HYPERBOLIC KINETICS AND THERMODYNAMICS OF IRREVERSIBLE PROCESSES

The hyperbolic dependence of flux on substrate activity of enzyme-catalyzed reactions is conventionally viewed in terms of saturation kinetics. As substrate is depleted in a closed irreversible reaction system, the process approaches equilibrium and flux declines to zero. The near-equilibrium domain can be described by the thermodynamics of irreversible processes (TIP; Prigogine, 1967) or nonequilibrium thermodynamics (NET; Katchalsky and Curran, 1967). For a general review and a specific discussion of hyperbolic kinetics versus linear flux/force relations see Westerhoff and van Dam (1987). Theoretical criteria for the expanded range of linearity have been developed by Gnaiger (1989). Here, oxygen dependence of mitochondrial respiration is analyzed in terms of interactions between molar Gibbs energy changes in the respiratory chain, proton/electron stoichiometries, and electrochemical potentials of H^+ transmembrane transport. The concept is illustrated for the specific case of mitochondrial respiration of succinate in the presence of rotenone and at maximum ATP/ADP ratios (Fig. 4).

Coupling of Input and Output Forces

The power input of oxidative phosphorylation results from catabolism (k) of reduced substrates and electron transport to O_2,

$$\text{k:} \quad O_2 + 2\ Suc^{2-} = 2\ Fum^{2-} + 2\ H_2O \qquad (6)$$

The partial Gibbs energy change per advancement of the reaction, $\partial G/\partial_k\xi_{O_2}$, is the Gibbs force, $\Delta_k G_{O_2}$ ($kJ \cdot mol^{-1}$), expressed per mol O_2 (Gnaiger, 1993b). The standard electromotive force, E^o, is 33 mV in the reduction of fumarate to succinate (Nicholls and Ferguson, 1992), corresponding to a standard Gibbs force of $\Delta_k G_{O_2}^o = -302$ $kJ \cdot mol^{-1}$ O_2 at a fumarate/succinate concentration ratio of 1. Reaction (6) is independent of pH. The standard pressure, $p^o_{O_2} = 101.325$ kPa (pure oxygen at 760 mm Hg), is unphysiological in tissues (Fig. 1) and is replaced here by a physiological standard of $p^*_{O_2} = 1$ kPa. The corresponding standard Gibbs force is less exergonic than $\Delta_k G_{O_2}^o$ by $RT \cdot \ln(101.325)$, i.e., -290 $kJ \cdot mol^{-1}$ O_2 at 25°C. The actual catabolic input force in reaction (6) incorporates the fumarate/succinate ratio and deviations from $p^*_{O_2}$,

$$\Delta_k G_{O_2} = -290 + RT \cdot \left(\ln \frac{[fum]^2}{[suc]^2} - \ln p_{O_2} \right) \qquad (7)$$

Coupled respiration pumps protons "uphill" from the negative matrix side across the inner mitochondrial membrane. The corresponding output force is the pro-

ton electrochemical potential, $\Delta\tilde{\mu}_{H^+}$ (kJ·mol^{-1} H$^+$). Analogous to the electromotive force, Mitchell defined the protonmotive force, $\mathbf{\Delta p} = -\Delta\tilde{\mu}_{H^+}/F$ (mV). A typical value for mitochondria at state 4 is −200 mV = 19.3 kJ·mol^{-1} H$^+$.

The ratio of protons translocated per O_2 consumed is a matter of continuing debate (Trumpower and Gennis, 1995). At a translocation stoichiometry of 14 H^+/O_2 for oxidation of succinate (Beavis, 1986), and a proton electrochemical potential of 19.3 kJ·mol^{-1} H$^+$, the Gibbs energy conserved in pumping protons against the gradient is 14·19.3 = 270 kJ·mol^{-1} O_2. In oxidative phosphorylation, this Gibbs energy is partly conserved in ATP, but it is dissipated when a static head of maximum ATP/ADP ratios is maintained at state 4. The effective force of mitochondrial respiration is the sum of the catabolic input force of oxygen consumption, $\Delta_k G_{O_2}$ (kJ·mol^{-1} O_2) [Eq. (7)], and the coupled output force of proton translocation times the H^+/O_2 stoichiometry. At 25°C and standard $p^*_{O_2}$, the net force of catabolic input (k) and H$^+$ translocation output (H) is $\Delta_{kH}G^*_{O_2}$,

$$\Delta_{kH}G^*_{O_2} = -290 + 11.4 \cdot \log \frac{[\text{fum}]}{[\text{suc}]} + H^+/O_2 \cdot \Delta\tilde{\mu}_{H^+} \quad (8)$$

where the asterisk indicates constant oxygen pressure of 1 kPa, without any other restrictions of standard states. The actual kH-coupled force, $\Delta_{kH}G_{O_2}$, is then expressed in terms of Eqs. (7) and (8) as a function of p_{O_2},

$$\Delta_{kH}G_{O_2} = \Delta_{kH}G^*_{O_2} - 5.7 \cdot \log p_{O_2} \quad (9)$$

This formalism for a coupled process remains valid for *serial* uncoupling (Gnaiger, 1993c), when proton translocation has actually taken place and energy is dissipated owing to serially linked processes (proton leak or slip through the ATP synthase). *Parallel uncoupling* by electron short-circuiting (redox slip; Pietrobon *et al.*, 1982) would abolish proton pumping and require a modification of the simple additive form of Eq. (8) (Westerhoff and van Dam, 1987; Groen *et al.*, 1990) but is of minor importance under the conditions of the present considerations (Luvisetto *et al.*, 1994; Brand *et al.*, 1994).

Fluxes and Forces at Low p_{O_2}

The net force of mitochondrial respiration is reduced to zero as oxygen declines. The theoretical minimum p_{O_2} can then be calculated from Eq. (9) at $\Delta_{kH}G_{O_2} = 0$,

$$p_{O_2}(\text{min}) = \exp(\Delta_{kH}G^*_{O_2}/RT) \quad (10)$$

For $\Delta_{kH}G^*_{O_2} = -20$ kJ·mol^{-1} [at $\mathbf{\Delta p} = -200$ mV, fum/suc = 1; or equivalent proton/redox electrochemical compensation; Eq. (8)] and $RT = 2.48$ kJ·mol^{-1} (25°C), the minimum p_{O_2} is 0.0003 kPa [Eq. (10)]. This is practically zero from an experimental point of view, and validates the assumptions for internal oxygen calibration applied above. The net Gibbs force of mitochondrial respiration [Eq. (8)] is sufficient to drive oxygen to extremely low pressures even at high membrane potentials. On the other hand, redox slip may render the effective net force less exergonic when fully reduced cytochrome *c* oxidase is reoxidized, a condition considered to be artificial with respect to physiological conditions (Babcock and Wikström, 1992; Malmström, 1993).

The kH-coupled (net) force in the oxidation of succinate at state 4 becomes less exergonic from −32 and −26 to −20 kJ·mol^{-1} O_2, as the p_{O_2} declines from 100 and 10 to 1 kPa at a fum/suc ratio of 1 and $\Delta\tilde{\mu}_{H^+} = 19.3$ kJ·mol^{-1} [Eq. (9)]. Considering the net rather than input force, the significant effect of p_{O_2} becomes obvious. Compensatory changes in the redox state at oxygen pressures as high as 10 kPa (100 μM O_2; Wilson *et al.*, 1979a) are expected from a thermodynamic but not a kinetic perspective, particularly since the membrane potential and pH gradient change very little even under short-term anoxic conditions (Andersson *et al.*, 1987). Small changes of the protonmotive force can compensate for shifts in redox state. For instance, a tenfold reduction of the fum/suc ratio is compensated by a change of the protonmotive force by only −8 mV (corresponding to a change of $\Delta\tilde{\mu}_{H^+}$ by 0.8 kJ·mol^{-1} H$^+$). Under the condition of such proton/redox electrochemical compensation the fum/suc ratio and $\Delta\tilde{\mu}_{H^+}$ in Eq. (8) are interdependent and yield a constant oxygen-independent component of the kH-coupled force [$\Delta_{kH}G^*_{O_2}$ in Eq. (9)]. Such compensation has in fact been observed in terms of changes of the phosphorylation potential ([ATP]/[ADP]·[P_i] which is coupled to the protonmotive force) behaving almost as a mirror image of the redox state (measured as cytochrome *c* reduction; Wilson *et al.*, 1979a). A stoichiometry of mitochondrial H$^+$ translocation of 16 H^+/O_2 (e.g., Costa *et al.*, 1984) yields an output force, $H^+/O_2 \cdot \Delta\tilde{\mu}_{H^+}$, of 309 kJ·mol^{-1} O_2 at a protonmotive force of −200 mV. The input force [Eq.

(7)] at a p_{O_2} of 1 kPa would have to amount to −329 kJ·mol^{-1} O_2 to yield again a $\Delta_{kH}G^*_{\delta_2}$ of −20 kJ·mol^{-1} O_2. The corresponding fum/suc ratio is calculated as 0.0004 from Eq. (7).

In conclusion, $\Delta_{kH}G^*_{\delta_2}$ equals approximately −20 kJ·mol^{-1} not only for the standard conditions assumed above, but this oxygen-independent component is maintained constant whenever a decrease of the fum/suc ratio is compensated by a corresponding increase of the proton electrochemical potential. When a p_{O_2} of 1 kPa is reached in a closed Oxygraph chamber with initial succinate concentration of 5 mM (Fig. 4), then 0.21 mM O_2 has been consumed and 0.08 mM fumarate plus 0.34 mM malate accumulated in the presence of rotenone. The corresponding fum/suc ratio is 0.02, and the catabolic input force at a p_{O_2} of 1 kPa is −310 kJ·mol^{-1} O_2 when measured in the extramitochondrial medium [Eq. (7)]. This is a maximum estimate since the intramitochondrial fum/suc ratio is higher without passive equilibration of these charged substances across the inner mitochondrial membrane. $\Delta_{kH}G^*_{\delta_2}$ would be maximally exergonic around −40 kJ·mol^{-1} O_2 at a protonmotive force of −210 mV and a H^+/O_2 ratio of 14, but would again amount to −20 kJ·mol^{-1} O_2 at a protonmotive force of −210 mV [$\Delta\tilde{\mu}_{H^+}$ = 20.7 kJ·mol^{-1}; Eqs. (8) and (9)] under the condition of proton/redox electrochemical compensation in the range of fum/suc ratios of 0.02–1.

In general, flux is a function of (1) a reaction coefficient, *b*, expressing the enzymatic activity, (2) a kinetic coefficient, α, related to effective substrate and product concentrations of the reaction, and (3) the driving force (molar Gibbs energy) of the reaction, Δ_rG_B, which is the thermodynamic component,

$$J_B = -b\cdot\alpha\cdot\Delta_rG_B \qquad (11)$$

Δ_rG_B is the net Gibbs force in the case of coupled processes ($\Delta_{kH}G_{O_2}$). The product $\alpha\cdot\Delta_rG_B$ yields the unit of (chemiosmotic) pressure and may be regarded as a generalized "reaction pressure" (Gnaiger, 1989). Flux/force linearity requires α to be constant, in which case the phenomenological conductivity, $L = b\cdot\alpha$, is constant and the "ergodynamic" equation (11) becomes identical to the flux/force relation of nonequilibrium thermodynamics (Katchalski and Curran, 1965). To test for linear flux/force relations of mitochondrial respiration at low p_{O_2}, flux can be related to the net force in terms of the oxygen-independent component, $\Delta_{kH}G^*_{\delta_2}$ [obtained experimentally as a parameter; Eq. (12)], and the logarithm of p_{O_2} (measured and treated as the independent variable),

$$J_{O_2} = -L\cdot(\Delta_{kH}G^*_{\delta_2} - 5.7\cdot\log p_{O_2}) \qquad (12)$$

A nonlinear fit of mitochondrial respiration and p_{O_2} on the basis of Eq. (12) in the low-oxygen range yields $\Delta_{kH}G^*_{\delta_2}$ = −18.1 kJ·mol^{-1} O_2 (Fig. 4; dashed line). The linear flux/force relation of Eq. (12) is plotted in Fig. 4 (inset), where the force, $\Delta_kG_{O_2}$, is calculated from Eq. (9) and $\Delta_{kH}G^*_{\delta_2}$ = −18.1 kJ·mol^{-1} O_2. This is well within the range of theoretically expected values of $\Delta_{kH}G^*_{\delta_2}$ for succinate respiration [Eq. (8)]. Hyperbolic saturation kinetics does not reproduce the modest increase of flux in the p_{O_2} range of 0.1–1 kPa (Fig. 4; full line). Without incorporating any saturation effect, on the other hand, Eq. (12) overestimates the dependence of flux on p_{O_2} between 0.1 and 1 kPa. Both models diverge to a larger extent if a higher range of p_{O_2} values is incorporated in the analysis. In the high-oxygen region of significant divergence, two mechanisms must be distinguished which are not mutually exclusive: (1) oxygen saturation of the system, and (2) regulation of $\Delta_{kH}G^*_{\delta_2}$ [Eq. (8)] to compensate for the effect of p_{O_2} and thus keep the net force [Eq. (9)] and hence flux constant (Wilson *et al.*, 1979).

The thermodynamic model of respiratory control by oxygen (Fig. 5) illustrates the relation between the

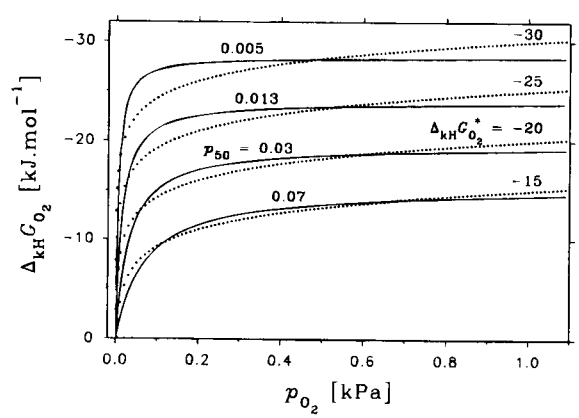

Fig. 5. Thermodynamic model of respiratory control by oxygen. Net Gibbs forces, $\Delta_{kH}G_{O_2}$ (dotted lines), were calculated as a function of p_{O_2} from Eq. (9) for various values of $\Delta_{kH}G^*_{\delta_2}$ (shown by numbers on the right; at physiological standard $p^*_{\delta_2}$ = 1 kPa). This kH-coupled Gibbs force, $\Delta_{kH}G^*_{\delta_2}$ (k: catabolic input force; H: proton translocation output force; superscript*: physiological standard oxygen pressure), was held constant for each plot over the p_{O_2} range shown, which is the case at constant redox potential, constant H^+/O_2 stoichiometry, and constant protonmotive force, and is also true under various conditions of proton/redox electrochemical compensation [Eq.(8)]. Hyperbolic fits (full lines) were calculated after converting the Gibbs force/p_{O_2} relations into data points (shown by dots), yielding apparent p_{50} values (shown by numbers on the left).

net force and p_{O_2} at different $\Delta_{kH}G^*_{\delta_2}$ values which are held constant over the p_{O_2} range considered. Plots of the kH-coupled force, $\Delta_{kH}G_{O_2}$, were calculated from Eq. (9) as a function of oxygen pressure for values of $\Delta_{kH}G^*_{\delta_2}$ from -15 to -30 kJ·mol^{-1} O_2 (Fig. 5). $\Delta_{kH}G_{O_2}$ can be treated to be proportional to flux [Eq. (12); dotted lines in Fig. 5] based on the experimentally observed linear flux/force relation (Fig. 4; inset) and under the assumption of proton/redox electrochemical compensation, at constant $\Delta_{kH}G^*_{\delta_2}$. Four remarkable properties emerge in comparison with our experimental data (Fig. 4) and in relation to the effect of uncouplers on p_{50} (Fig. 3 and Table I). (1) Near-hyperbolic relations are obtained in the oxygen control range (Fig. 5; dotted lines). (2) The deviation from the hyperbolic function yields a similar pattern as observed experimentally (Fig. 4), explaining the dependence of apparent p_{50} from the p_{O_2} range chosen for curve fitting (compare Fig. 2). (3) In the theoretical $\Delta_{kH}G^*_{\delta_2}$ range of -15 to -25 kJ·mol^{-1} O_2, predictions of Eq. (12) can be fitted by a hyperbolic function and yield apparent p_{50} values in the range of 0.013–0.07 kPa (Fig. 5; full lines), in agreement with experimental results (Fig. 4). (4) The apparent p_{50} values calculated from the hyperbolic fits decline with increasing (exergonic) net Gibbs forces, steeply when $\Delta_{kH}G^*_{\delta_2}$ is more exergonic than -25 kJ·mol^{-1} O_2 (Fig. 5). This explains the very low p_{50} values reported for uncoupled mitochondria (<0.005 kPa; Table I) and the decrease of p_{50} in uncoupled and inhibited cells (Fig. 3). It is well established that the proton electrochemical potential collapses in response to protonophores such as FCCP, with the effect of a more exergonic value of $\Delta_{kH}G^*_{\delta_2}$ [Eq. (8)].

CONCLUSIONS

Understanding the role of oxygen is not merely of theoretical interest in bioenergetics but has broad implications for normoxic mitochondrial function and clinical diagnostics and intervention strategies. The current view of mitochondrial function is partly biased owing to the notoriously high p_{O_2} range in most mitochondrial *in vitro* experiments. Specifically, the low flux control coefficient of cytochrome *c* oxidase (Groen *et al.*, 1982) needs re-evaluation under physiological normoxic p_{O_2}, that is, at a mitochondrial p_{O_2} < 1 kPa.

For the first time, the hyperbolic oxygen dependence of mitochondrial respiration was deduced from the thermodynamics of irreversible processes, rationalizing the low p_{50} values of coupled mitochondria and the decrease of the p_{50} upon uncoupling. The kinetic and thermodynamic models are equivalent (in the sense of Westerhoff and van Dam, 1987) as far as the curve-fitting power is concerned. However, the mechanisms deduced from the two descriptions are different. The kinetic model of respiratory oxygen dependence (Chance *et al.*, 1985; Wilson *et al.*, 1979a and b) assumes saturation of the enzyme system, whereas thermodynamic flux/force relations explain the kinetic saturation phenomenon in terms of a logarithmic p_{O_2} dependence of the flux [Eq. (12)]. A mathematically similar pattern is explained from different perspectives.

Biological energy transformations are complex. A quantitative analysis of their control and regulatory mechanisms requires a multitude of experimental approaches and the conceptual input of catalysis, kinetics, and thermodynamics. Their reconciliation [Eq. (11)] presents one of the major challenges in bioenergetics. Flux control analysis demonstrates that control may be distributed democratically over a multitude of enzymes in a pathway rather than being confined to a monarchical rate-controlling step. In analogy, unification of kinetic and thermodynamic analysis (which is not yet achieved) discloses a view on metabolism where flux control by allosteric modulation of enzymes, kinetically saturable concentrations, and Gibbs forces are not mutually exclusive but constitute an ensemble of mechanisms acting in concert.

ACKNOWLEDGMENTS

We thank Mag. M. Reck for excellent collaboration in the software development (DatLab). This work was supported by the Austrian Science Foundation, FWF project No. P7162-BIO, and a project of the Austrian Ministry of Science.

REFERENCES

Andersson, B. S., Yee Aw, T., and Jones, D. P. (1987). *Am. J. Physiol.* **252**, C349–C355.
Arthur, P. G., Hogan, M. C., Bebout, D. E., Wagner, P. D., and Hochachka, P. W. (1992). *J. Appl. Physiol.* **73**, 737–742.
Babcock, G. T., and Wickström, M. (1992). *Nature* **356**, 301–309.
Beavis, A., D. (1986). *J. Biol. Chem.* **262**, 6165–6173.
Brand, M. D., Chien, L.-F., and Diolez, P. H. (1994). In *What is Controlling Life?* (Gnaiger, E., Gellerich, F. N., and Wyss, M., eds.), *Modern Trends in BioThermoKinetics*, Vol. 3, Innsbruck University Press, Innsbruck, pp. 125–128.
Brown, G. C., and Cooper, C. E. (1994). *FEBS Lett.* **356**, 295–298.
Chance, B. (1965). *J. Gen. Physiol.* **49**, 163–188.

Chance, B., Leigh, J. S., Clark, B. J., Maris, J., Kent, J., Nioka, S., and Smith, D. (1985). *Proc. Natl. Adad. Sci. USA* **82**, 8384–8388.

Chinet, A. E., and Mejsnar, J. (1989). *J. Appl. Physiol.* **66**, 253–260.

Cole, R. C., Sukanek, P. C., Wittenberg, J. B., and Wittenberg, B. A. (1982). *J. Appl. Physiol.* **53**, 1116–1124.

Connett, R. J., Gayeski, T. E. J., and Honig, C. R. (1985). In *Oxygen Transport to Tissue,* Vol. VII (Kreuzer, F., Cain, S. M., Turek, Z., and Goldstick, T. K., eds.), Plenum Press, New York, pp. 291–300.

Costa, L. E., Reynafarje, B., and Lehninger, A. L. (1984). *J. Biol. Chem.* **259**, 4802–4811.

Degn, H., and Wohlrab, H. (1971). *Biochim. Biophys. Acta* **245**, 347–355.

Dionne, K. E. (1990). *J. Biol. Chem.* **265**, 15400–15402.

Einarsdóttir, Ó. (1995). *Biochim. Biophys. Acta* **1229**, 129–147.

Ferreira, J. (1992). *Eur. J. Biochem.* **207**, 857–866.

Froncisz, W., Lai, C.-S., and Hyde, J. S. (1985). *Proc. Natl. Acad. Sci. USA* **82**, 411–415.

Gayeski, T. E. J., and Honig, C. R. (1986). *Am. J. Physiol.* **251**, H789–H799.

Gayeski, T. E. J., and Honig, C. R. (1991). *Am. J. Physiol.* **260**, H522–H531.

Gnaiger, E. (1983). In *Polarographic Oxygen Sensors. Aquatic and Physiological Applications* (Gnaiger, E., and Forstner, H., eds.), Springer, Berlin, Heidelberg, New York, pp. 134–166.

Gnaiger, E. (1989). In *Energy Transformations in Cells and Organisms* (Wieser, W., and Gnaiger, E., eds.), Thieme, Stuttgart, pp. 6–17.

Gnaiger, E. (1993a). In *The Vertebrate Gas Transport Cascade: Adaptations to Environment and Mode of Life* (Bicudo, J.E.P.W., ed.), CRC Press, Boca Raton, Ann Arbor, London, Tokyo, pp. 358–370.

Gnaiger, E. (1993b). *Pure Appl. Chem.* **65**, 1983–2002.

Gnaiger, E. (1993c). In *Surviving Hypoxia: Mechanisms of Control and Adaptation* (Hochachka, P. W., Lutz, P. L., Sick, T., Rosenthal, M., and Van den Thillart, G., eds.), CRC Press, Boca Raton, Ann Arbor, London, Tokyo, pp. 77–109.

Groen, A. K., Wanders, R. J. A., Westerhoff, H. V., van der Meer, R., and Tager, J. M. (1982). *J. Biol. Chem.* **257**, 2754–2757.

Groen, B. H., Berden, J. A., and Van Dam, K. (1990). *Biochim. Biophys. Acta* **1019**, 122–127.

Hale, J. M. (1983). In *Polarographic Oxygen Sensors, Aquatic and Physiological Applications.* (Gnaiger, E., and Forstner, H., eds.), Springer, Berlin, Heidelberg, New York, pp. 3–17.

Haller, T., Ortner, M., and Gnaiger, E. (1994). *Anal. Biochem.* **218**, 338–342.

Jöbsis, F. F. (1972). *Fed. Proc.* **5**, 1404–1413.

Jones, D. P. (1986). *Am. J. Physiol.* **250**, C663–C675.

Jones, D. P., and Kennedy, F. G. (1982). *Am. J. Physiol.* **243**, C247–C253.

Jones, D. P., and Mason, H. S. (1978). *J. Biol. Chem.* **253**, 4874–4880.

Kadenbach, B. (1986). *J. Bioenerg. Biomembr.* **18**, 39–54.

Katchalsky, A., and Curran, P. F. (1965). *Nonequilibrium Thermodynamics in Biophysics,* Harvard University Press, Cambridge, Massachusetts.

Kennedy, F. G., and Jones, D. P. (1986). *Am. J. Physiol.* **250**, C374–C383.

Kreutzer, U., and Jue, T. (1995). *Am. J. Physiol.* **268**, H1675–H1681.

Luvisetto, S., Canton, M., Schmehl, I., and Azzone, G. F. (1994). In *What is Controlling Life?* (Gnaiger, E., Gellerich, F. N., and Wyss, M., eds.), *Modern Trends in BioThermoKinetics,* Vol. 3, Innsbruck University Press, Innsbruck, pp. 122–124.

Malmström, B. G. (1993). *Acc. Chem. Res.* **26**, 332–338.

Méndez, G., and Gnaiger, E. (1994). In *What is Controlling Life?* (Gnaiger, E., Gellerich, F. N., and Wyss, M., eds.), *Modern Trends in BioThermoKinetics,* Vol. 3, Innsbruck University Press, Innsbruck, pp. 191–194.

Mertens, S., Noll, T., Spahr, R., Krutzfeldt, A., and Piper, H. M. (1990). *Am. J. Physiol.* **258**, H689–H694.

Nicholls, D. G., and Ferguson, S. J. (1992). *Bioenergetics 2,* Academic Press, London.

Nicholls, P. (1993). In *Modern Trends in BioThermoKinetics* (Schuster, S., Rigoulet, M., Ouhabi, R., and Mazat, J. P., eds.), Plenum Press, New York, London, pp. 11–16.

Petersen, L. C., Nicholls, P., and Degn, H. (1974). *Biochem. J.* **142**, 247–252.

Pietrobon, D., Zoratti, M., Azzone, G. F., Stucki, J. W., and Walz, D. (1982). *Eur. J. Biochem.* **127**, 483–494.

Prigogine, I. (1967). *Introduction to Thermodynamics of Irreversible Processes,* Interscience, New York, 3rd edn.

Reynafarje, B., Costa, L. E., and Lehninger, A. L. (1985). *Anal. Biochem.* **145**, 406–418.

Robiolio, M., Rumsey, W. L., and Wilson, D. F. (1989). *Am. J. Physiol.* **256**, C1207–C1213.

Rumsey, W. L., Schlosser, C., Nuutinen, E. M., Robiolio, M., Wilson, D. F. (1990). *J. Biol. Chem.* **265**, 15392–15399.

Schindler, F. J. (1967). In *Methods in Enzymology,* Vol. 10 (Estabrook, R., and Pullman, M. E., eds.), pp. 629–634.

Schumacker, P. T., Chandel, N., and Agusti, A. G. N. (1993). *Am. J. Physiol.* **265**, L395–L402.

Sugano, T., Oshino, N., and Chance, B. (1974). *Biochim. Biophys. Acta* **347**, 340–358.

Starlinger, H., and Luebbers, D. W. (1972). *Pfluegers Arch.* **337**, 19–28.

Steinlechner, R., Eberl, T., Margreiter, R., and Gnaiger, E. (1994). In *What is Controlling Life?* (Gnaiger, E., Gellerich, F. N., and Wyss, M., eds.), *Modern Trends in BioThermoKinetics,* Vol. 3, Innsbruck University Press, Innsbruck, pp. 283–287.

Tamura, M., Hazeki, O., Nioka, S., and Chance, B. (1989). *Annu. Rev. Physiol.* **51**, 813–834.

Trumpower, B., L., and Gennis, R. B. (1995). *Annu. Rev. Biochem.* **63**, 675–716.

Weibel, E. R. (1984). *The Pathway for Oxygen. Structure and Function in the Mammalian Respiratory System,* Harvard University Press, Cambridge, Massachusetts.

Westerhoff, H. V., and Van Dam, K. (1987). *Thermodynamics and Control of Free-Energy transduction,* Elsevier, Amsterdam.

Wilson, D. F., Erecińska, M., Drown, C., and Silver, I. A. (1979a). *Arch. Biochem. Biophys.* **195**, 485–493.

Wilson, D. F., Owen, C. S., and Erecińska, M. (1979b). *Arch. Biochem. Biophys.* **195**, 494–504.

Wilson, D. F., Rumsey, W. L., Green, T. J., and Vanderkooi, J. (1988). *J. Biol. Chem.* **263**, 2712–2718.

Wittenberg, B. A., and Wittenberg, J. B. (1985). *J. Biol. Chem.* **260**, 6548–6554.

Wittenberg, B. A., and Wittenberg, J. B. (1989). *Annu. Rev. Physiol.* **51**, 857–878.